Synergy of electronic and nuclear energy losses on the extended defects kinetics in UO2 by using in situ TEM

M. Bricout, G. Gutierrez, C. Baumier, C. Bachelet, D. Drouan, F. Garrido, C. Onofri

▶ **To cite this version:**

M. Bricout, G. Gutierrez, C. Baumier, C. Bachelet, D. Drouan, et al.. Synergy of electronic and nuclear energy losses on the extended defects kinetics in UO2 by using in situ TEM. J.Nucl.Mater., 2021, 554, pp.10.1016/j.jnucmat.2021.153088. 10.1016/j.jnucmat.2021.153088 . hal-03260023

HAL Id: hal-03260023
https://hal.science/hal-03260023v1

Submitted on 19 Jul 2022

HAL is a multi-disciplinary open access archive for the deposit and dissemination of scientific research documents, whether they are published or not. The documents may come from teaching and research institutions in France or abroad, or from public or private research centers.

L'archive ouverte pluridisciplinaire **HAL**, est destinée au dépôt et à la diffusion de documents scientifiques de niveau recherche, publiés ou non, émanant des établissements d'enseignement et de recherche français ou étrangers, des laboratoires publics ou privés.

Synergy of electronic and nuclear energy losses on the extended defects kinetics in UO_2 by using *in situ* TEM

M. Bricout[1], G. Gutierrez[1], C. Baumier[2], C. Bachelet[2], D. Drouan[3], F. Garrido[2], C. Onofri[3]*

[1] Université Paris-Saclay, CEA, Service de Recherches de Métallurgie Physique, 91191, Gif-sur-Yvette, France

[2] Laboratoire de Physique des 2 infinis Irène Joliot-Curie (IJCLab), Université Paris-Saclay, Orsay, France

[3] CEA, DES, IRESNE, DEC, Cadarache, F-13108 St Paul lez Durance, France

Abstract

During in reactor operations, the slowing down of the fission fragments generates most of the damage in uranium dioxide. Theses latter deposit their energy to both atomic and electronic subsystems through nuclear and electronic interactions. To study the possible synergistic effects of nuclear and electronic energy deposition on the microstructure, UO_2 thin foils have been irradiated with 0.39 MeV Xe and/or 6 MeV Si ions at 298 K by single or dual ion beam irradiation. The evolution of extended defects was characterized by *in situ* Transmission Electron Microscopy. It appears that, whatever the ion beam used, a similar evolution with fluence increase is observed: a nucleation of small dislocation loops, which increase in density up to a saturation value, then the average loop size increases. However, the kinetics change according to the irradiation conditions. In the case of the dual beam irradiation, all the phenomena occur at a lower value of damage level. The local increase of the temperature along the 6 MeV Si ion path seems to lead to an enhanced defect mobility, as in the case of irradiations performed in temperature.

Keywords: UO_2, *in situ* TEM, extended defects, dual ion beam irradiation

*Corresponding author

E-mail: claire.onofri@cea.fr

1. Introduction

The uranium dioxide (UO_2) is commonly used as nuclear fuel for pressurized water reactors. During in-pile irradiation, it is simultaneously subjected to neutrons, fission fragments (FF), alpha, beta and gamma particles, as well as alpha recoils. Defects, such as cavities or dislocations, are mainly produced by the slowing down of the FF which have a kinetic energy ranging from 70 to 100 MeV. To investigate the involved mechanisms for defect production without having to deal with a highly radioactive matter, intensive investigations of the fuel modification by ion irradiations have been performed for many decades on UO_2 depleted pellets. The energetic ions deposit their energy to both atomic and electronic subsystems through nuclear or electronic interactions. Up to now, most of the studies on the irradiation effects in UO_2 have investigated either the formation of defects such as cavities and/or dislocations loops and lines by performing low-energies ion irradiations [1–9]; or the formation of a continuous ion track by ionization and electronic excitations for the high energy range (for electronic energy loss higher than 20 keV/nm [10, 11]) [10, 12–14]. While interactions between energetic ions and target nuclei lead to atomic displacements through elastic collisions, electronic energy deposition in UO_2 can cause localized temperature increase due to the electron-phonon coupling. The electronic energy deposition can thus affect the damage build up kinetics induced by nuclear energy losses. Recent works in other semiconductors such as Si, SiC, MgO, ZrO_2, $KTaO_3$ or borosilicates glasses have shown that electronic energy loss can either substantially reduce defects production, and thus affect the microstructural evolution, or enhance the damage production rate [15–22]. In UO_2, very few studies were interested in the coupling effect. High-energy irradiations were performed at high temperature (higher than 873 K) on pre-implanted samples with Xe ions to study the migration behavior of the implanted Xe under ionizations [23, 24]. It highlights that high-energy irradiations coupled with temperature lead to modifications of the UO_2 microstructure. In another study, a strain relaxation due to ionization has also been shown under dual ion beam irradiation [25]. In addition, an evolution from dislocation loops, generated by low-energy ion irradiation, to dislocation lines has been shown under dual beam irradiation compared to single beam irradiation at a given value of nuclear damage [26]. However, in this work, only an advanced state in terms of ion fluence has been characterized and the detailed microstructural evolution under ionization has not been reported. Thus a detailed study is required to understand the underlying mechanisms.

The current work aims to determine the synergy of electronic and nuclear energy losses on the extended defects kinetics in UO_2. It reports some results on *in situ* transmission electron microscopy (TEM) observations of polycrystalline UO_2 thin foils irradiated with low energy (0.39 MeV Xe) and/or “high”-energy (6 MeV Si) ions. Single, sequential, and dual-beam ion irradiations at room temperature (293 K) were performed at the JANNuS Orsay facility.

2. Experimental procedures

Polycrystalline UO_2 pellets of an average grain size of 7.6 µm and a density of 98% of the theoretical one (i.e. 10.952 g/cm^3) are cut to discs using a saw equipped with a diamond wire. Discs are further polished on one side down to a thickness of 500 µm and annealed under an Ar-H_2 (5%) gas mixture at 1700 °C for 24 h. After that, they are polished with colloidal silica suspension to reduce effects due to grain boundaries. Finally, they are annealed under the same Ar-H_2 (5%) atmosphere at 1400 °C for 4 h to maintain their stoichiometry (O/U = 2.00) [27] and to remove the last damage induced by polishing. A mechanical thinning on the rough face using the tripod polishing technique and a chemical etching [28] are finally applied to obtain thin foils of UO_2 with electron transparent zones.

The thickness (t) of the samples is determined through Electron Energy Loss Spectrometry (EELS) using a GIF TRIDIEM GATAN. We used a value of the collection semi-angle equal to 11.81 mrad. Thickness is deduced from the log-ratio method using the following formula [29]:

$$t = \lambda \ln\left(\frac{I_T}{I_0}\right)$$

where I_T is the total intensity of the EELS spectrum, I_0 the intensity of the zero-loss peak, and λ the electron mean free path for inelastic scattering [30]. Data are acquired using Gatan Digital Micrograph software. The mean thicknesses of the areas studied are about 40 nm. Uncertainties for sample thickness are set to 10 % [31].

In situ irradiations at 293 K are performed at the JANNuS-Orsay facility using the IRMA and the ARAMIS implanters [32]. Various irradiations were performed:

- Two single beam irradiations are carried out with either 0.39 MeV Xe^{3+} ion beam up to 1×10^{15} Xe/cm² or 6 MeV Si^{3+} ion beam up to 5×10^{14} Si/cm².
- One sample is also pre-implanted with 0.39 MeV Xe^{3+} ion beam at a fluence of 5×10^{14} Xe/cm² and further irradiated with 6 MeV Si^{3+} ion beam up to a fluence of 3×10^{14} Si/cm² (referred to as Xe then Si).
- Finally, the corresponding dual-beam irradiation (referred to as Xe & Si) is conducted to study the possible coupled effect between these two ion beams.

The flux of both ion beams is limited to about 8×10^{10} ions/(cm^2.s) to avoid the target heating. During the dual ion beam irradiation (Xe & Si), the flux ratio between Si and Xe ion beams is kept at a value of 2.

Irradiation parameters, plotted in fig. 1, are calculated using the SRIM code via the full cascade calculation mode [33]. The threshold displacement energies for U and O are set to 40 and 20 eV, respectively [34, 35]. The energy of the Si and the Xe ions are selected to major either electronic ($(dE/dx)_{elec}$) or nuclear ($(dE/dx)_{nucl}$) energy deposition. The 0.39 MeV Xe ion beam is used to induce nuclear damage into the sample, whereas the 6 MeV Si ions favor mainly electronic ionizations by inelastic collisions. The associated nuclear damage by 6 MeV Si ions in the thin foil is negligible for the studied fluence range (fig. 1(b)). It should be noted that this ion beam was the most energetic ion available at the JANNuS Orsay facility.

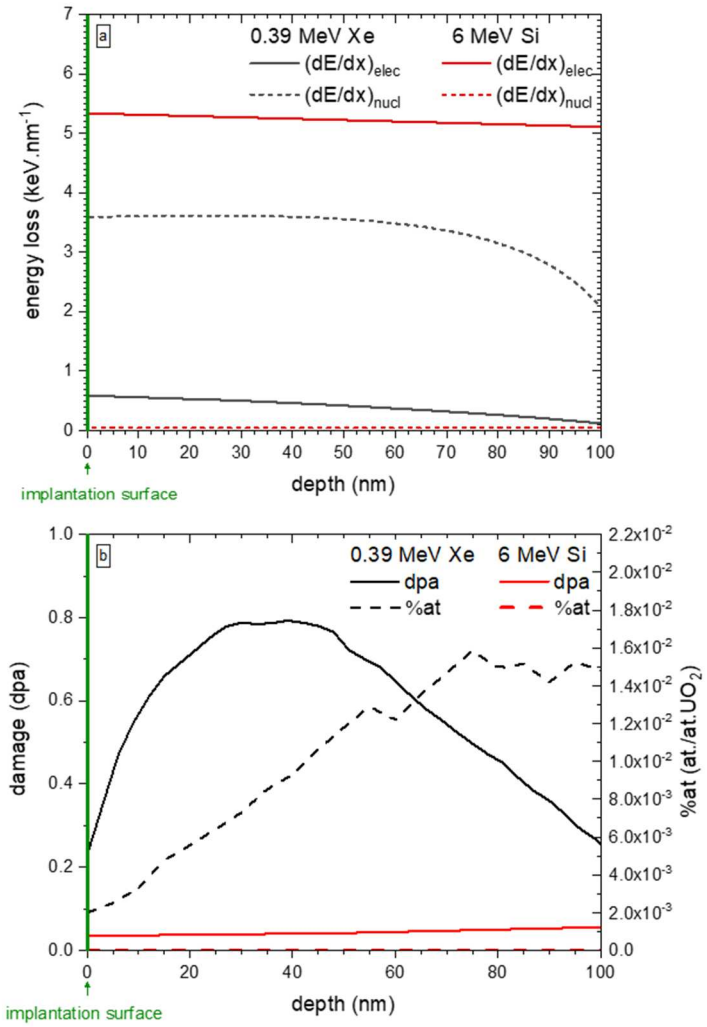

Figure 1: (a) Electronic ($(dE/dx)_{elec}$) and nuclear ($(dE/dx)_{nucl}$) energy losses depth profiles of 0.39 MeV Xe and 6 MeV Si in UO_2 and (b) atomic displacements and ion distribution at a fluence of 1×10^{14} at/cm² calculated with the SRIM software [33].

The irradiation conditions are summarized in table 1.

Table 1: Irradiation conditions for the Xe and the Si ion beams. The nuclear and electronic energy losses correspond to the mean value on the lamella thickness (t ≈ 40 nm).

Ion	Xe^{3+}	Si^{3+}
Energy (MeV)	0.39	6
$(dE/dx)_{elec}$ (keV/nm)	0.3	5.2
$(dE/dx)_{nucl}$ (keV/nm)	3.1	0.05
$\frac{\left(\frac{dE}{dx}\right)_{elec}}{\left(\frac{dE}{dx}\right)_{nucl}}$	0.1	104

In situ TEM characterizations are carried out during the irradiation with a 200 kV TECNAI G² 20 Twin TEM (spatial resolution of 0.27 nm, LaB_6 electron source) equipped with a GATAN ES500W 1k x 1k and an ORIUS 200 GATAN 2k x 2k CCD cameras. The loop densities and mean sizes are measured with the ImageJ software, from the characterization of between 30

and 400 loops per irradiation fluence, with diffraction vector *g* along with the <111> directions. As the observed dislocation loops have often an elliptical shape, their size is defined as the length of their longest axis. Uncertainty for dislocation loops densities is determined using the following formula:

$$\Delta d_{loop} \approx d_{loop} \sqrt{(\frac{1}{\sqrt{N}})^2 + (\frac{\Delta t}{t})^2}$$

Where d_{loop} is the loop density, N the number of counted loops, and t the thickness of the studied area, determined by EELS. The uncertainty of loop size is around 15% for all irradiation conditions, after considering this formula:

$$\Delta \emptyset_{loop} \approx \emptyset_{loop} \sqrt{(\frac{1}{\sqrt{N}})^2 + (\frac{\Delta px}{\emptyset_{loop}})^2}$$

Where $\emptyset_{loop}$ is the average loop size, N the number of measured loops, and Δpx the relative pixel error, set to 2 px based on our feedback.

3. Results

In this work, we focus on the coupling of electronic and atomic processes on the extended defect evolution. We will first investigate the role of the single-ion beams on the microstructure evolution to determine the influence of either the electronic or the nuclear energy losses. Then, we will discuss the synergetic effect between electronic and nuclear energy losses. This second part will present the results obtained on the ionization effect in a pre-damaged sample with Xe ions (Xe then Si) and on the simultaneous irradiation of Xe and Si ions (Xe & Si).

3.1. Separated effect of ballistic and electronic damage: single ion beam irradiations

3.1.1. 0.39 MeV Xe ions irradiation

The microstructural evolution is followed during irradiation with the video monitoring available on-site. Fig. 2 shows the bright field (BF) TEM images of the irradiated thin foil with 0.39 MeV Xe ions at 293 K at various fluences (up to 1×10^{15} Xe/cm²), recorded with diffraction vectors along with the <111> directions. The unirradiated thin foil does not exhibit any extended defects at the TEM scale (fig. 2(a)). No microstructural change is observed up to 6×10^{12} Xe/cm² (~0.04 dpa) (fig. 2(b)). Then, at 1×10^{13} Xe/cm² (~0.07 dpa), small black dots (some of them present black/white contrasts) of few nanometers appear as illustrated in fig. 2(c). These black dots are assigned to small dislocation loops, as observed in previous studies [2, 7, 36]. For higher fluences, more and more dislocation loops are observed (fig. 2(d-e)). Between 1×10^{14} (~0.7 dpa) and 5×10^{14} (~3.5 dpa), the loops size increases (fig. 2(e-f)). They present clearly the

contrast of larger loops well-defined. Between 5×10^{14} (~3.5 dpa) and 1×10^{15} Xe/cm² (~7 dpa), the microstructure evolved from dislocation loops to lines (fig. 2(f and g)).

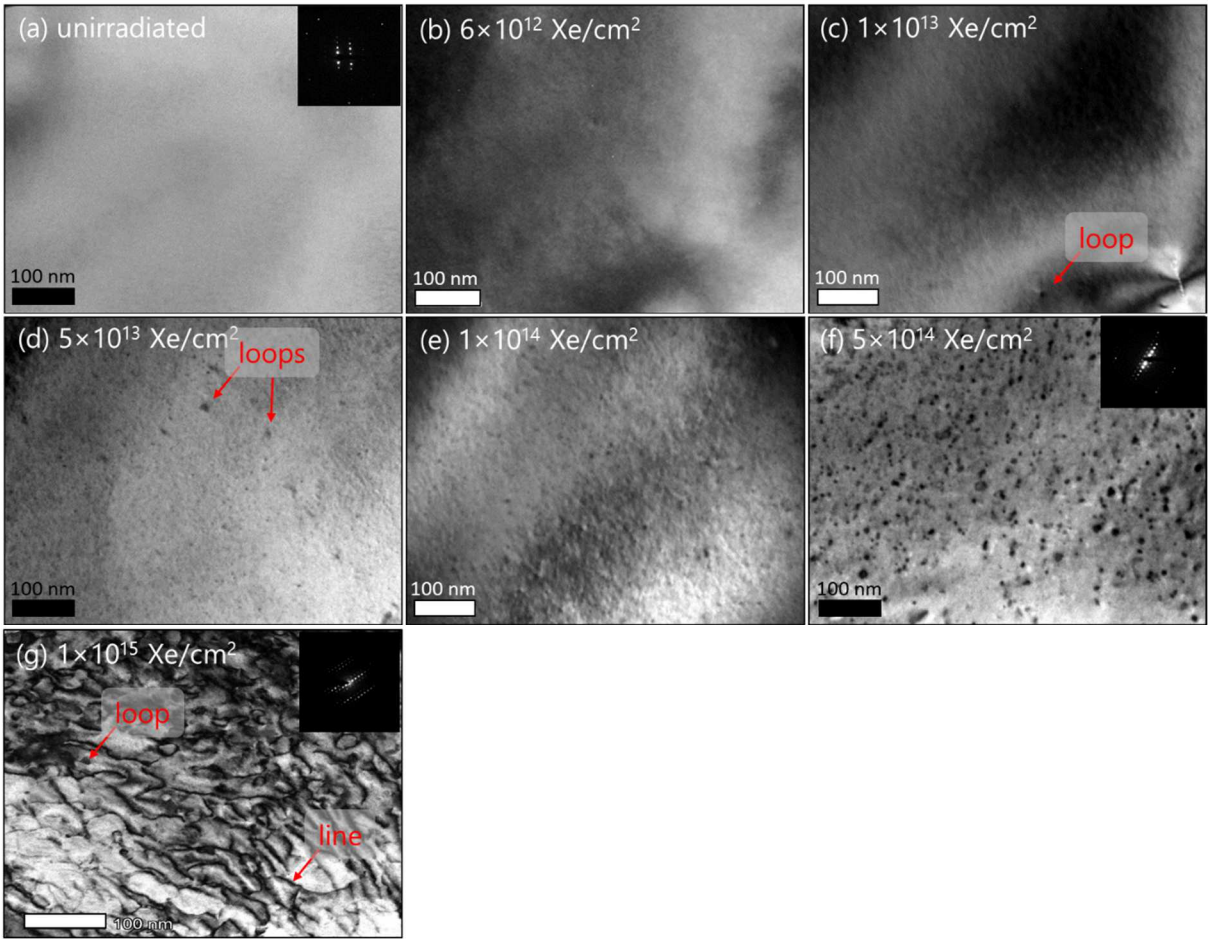

Figure 1: BF TEM images of polycrystalline UO_2 thin foil (a) unirradiated and irradiated at 293 K with 0.39 MeV Xe ions at (b) 6×10^{12}, (c) 1×10^{13}, (d) 5×10^{13}, (e) 1×10^{14}, (f) 5×10^{14} and (g) 1×10^{15} Xe/cm². The insets show the diffraction pattern along the <111> direction. The red arrow highlights the dislocation loops.

The dislocation loops density and the average loops size as a function of fluence were extracted from these micrographs (fig. 3).

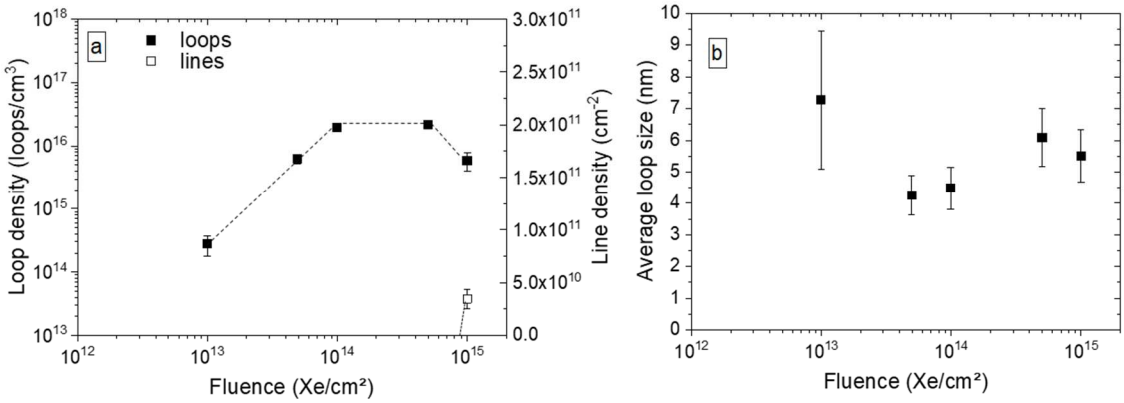

Figure 3: Evolution of (a) dislocation loop density (black scatters) and dislocation line density (white scatters) and (b) average loop size as a function of fluence after irradiation with 0.39 MeV Xe at 293 K. The represented values are obtained with a diffraction vector along the <111> directions. The dotted lines are guides for the eyes.

At 1×10^{13} Xe/cm², a low density of dislocation loops is highlighted. It has to be noted that, for these fluences, only 30 loops have been measured inducing a higher uncertainty and an overestimation of their size. With the irradiation fluence increase, the dislocation loop density increases up to 1×10^{14} Xe/cm² while their size remains constant at about 4 nm. For fluences ranging between 1 and 5×10^{14} Xe/cm², the loop density seems to saturate at around 2×10^{16} loops/cm^3 and the loop mean size tends to increase (up to 7 nm). At a fluence of 1×10^{15} Xe/cm², the microstructure exhibits dislocation lines (3.5×10^{10} cm^{-2}) and small dislocation loops (5.9×10^{15} loops/cm^3) between the lines with an average size of about 4 nm.

Fig. 4 shows the repartition of the dislocation loop size for fluences higher than 5×10^{13} Xe/cm². The two lowest fluences are not represented in this figure due to a non-statistical representation of their size because of the number of observed loops.

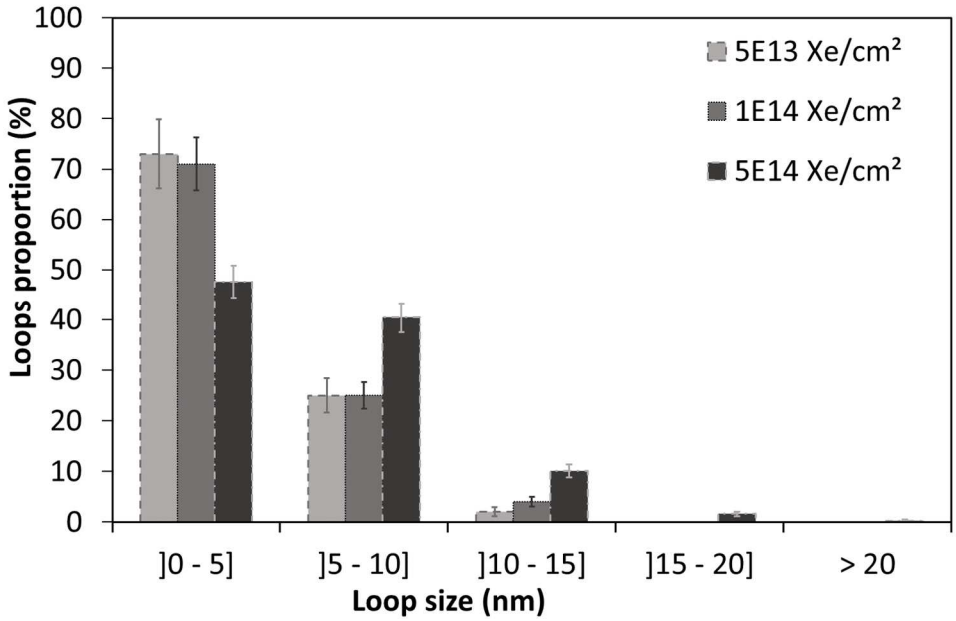

Figure 4: Repartition of the dislocation loop size at the various fluences induced by implantation with 0.39 MeV Xe at 293 K.

For fluences ranging between 5×10^{13} and 1×10^{14} Xe/cm², the loop proportion, whose sizes are lower than 10 nm, remains constant. The proportion of loops, whose sizes are between 10 and 15 nm, slightly increases ((2 ± 1) % for 5×10^{13} Xe/cm^2 and (4 ± 1) % for 1×10^{14} Xe/cm^2). At a fluence of 5×10^{14} Xe/cm², a significant increase of the number of the largest loops (+ 15 % for]5-10] nm and + 6 % for]10-15] nm), as well as a decrease of the number of the smallest loops (- 23 % for a size lower than 5 nm) are highlighted. A new size range appears (]15-20 nm]). At this fluence, 12 % of the observed loops achieve a diameter higher than 10 nm against 4 % at 1×10^{14} Xe/cm². A loop growth above 1×10^{14} Xe/cm² is thus clearly highlighted.
The evolution of loop size and density is consistent with previous studies [2, 3, 7, 36–38]. Dislocation loops evolve into dislocation lines after the loop density saturation and a loop growth.

3.1.2. 6 MeV Si ions irradiation

In situ analysis is also carried out for the UO_2 thin foil irradiated with 6 MeV Si ions to determine the influence of the electronic energy deposition (Fig. 5).

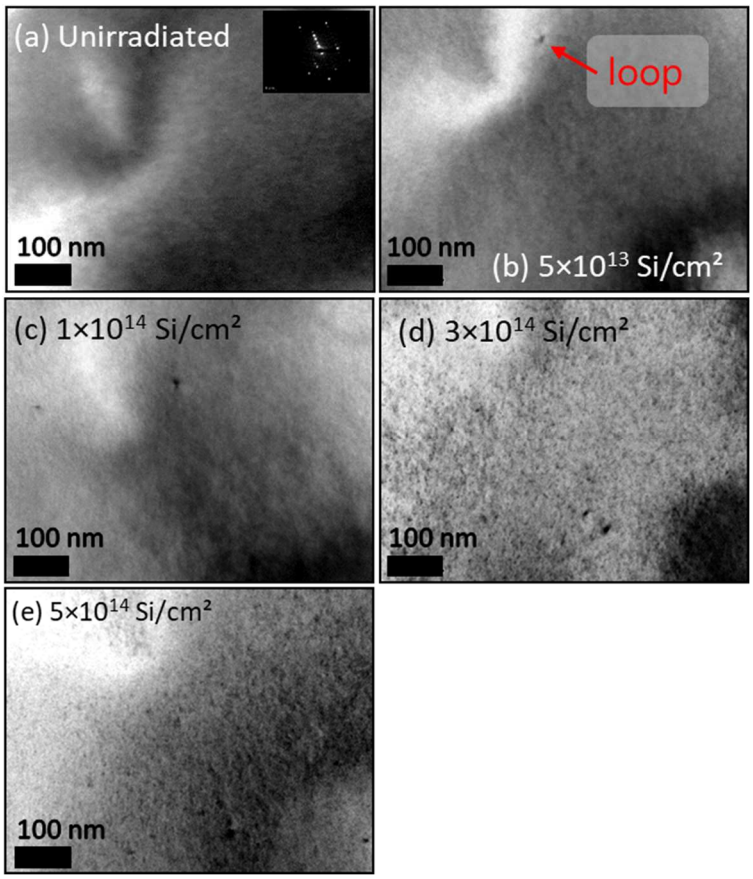

Figure 5: BF TEM images of polycrystalline UO_2 thin foil (a) unirradiated and irradiated at 293 K with 6 MeV Si ions at (b) 5×10^{13}, (c) 1×10^{14}, (d) 3×10^{14}, and (e) 5×10^{14} Si/cm^2. The inset shows the diffraction pattern along the <111> direction. The red arrow highlights the dislocation loop.

Before the irradiation, no defects are exhibited at the TEM scale (Fig. 5(a)). For lower fluence than 5×10^{13} Si/cm^2 (~ 0.005 dpa), no significant change is observed. Beyond this fluence, few dislocation loops at very low density (< 10^{15} loops/cm^3) are observed (Fig. 5(b-c)). At 3×10^{14} Si/cm^2 (~ 0.03 dpa), the observed loops density, of average size ~ 4 nm, reaches a value of 2×10^{15} loops/cm^3 (fig. 5(d)). For higher fluences, the dislocation loops begin to appear at a significant density (Fig. 5(e) – (2.4 ± 0.2) $\times10^{16}$ loops/cm^3). In conclusion, up to a fluence of 3×10^{14} Si/cm^2 (~ 0.03 dpa), the 6 MeV Si ions induce a small effect on the sample microstructure at the TEM scale. After 3×10^{14} Si/cm^2, too many dislocation loops are formed due to the 6 MeV Si irradiation. As it may disturb the microstructural evolution for dual-beam irradiation, the simultaneous irradiation was performed up to 2×10^{14} Si/cm^2.

3.1.3. Comparison between 0.39 MeV Xe and 6 MeV Si

To compare the two single ion beam irradiations, the loop evolution in terms of density and size is represented in fig. 6 as a function of the average damage level (dpa) determined on the lamella thickness (t ≈ 40 nm).

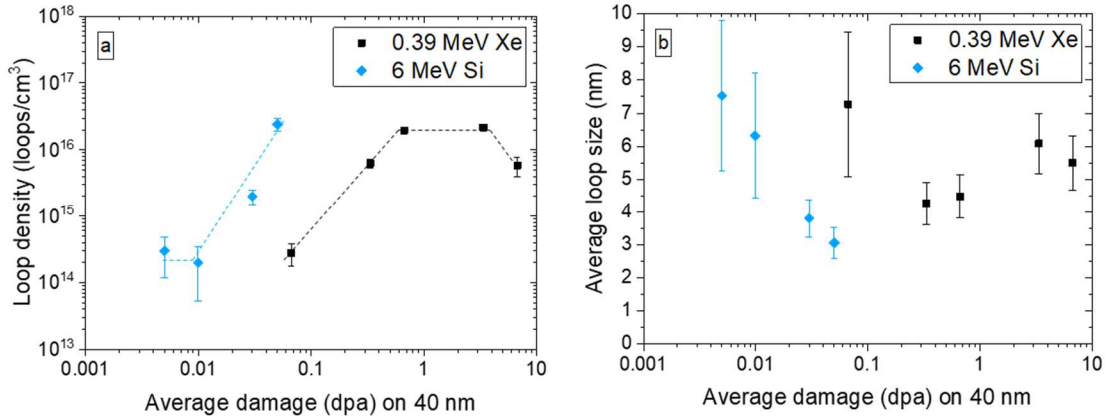

Figure 6: Evolution of (a) dislocation loop density and (b) loop size as a function of the average damage on the thin foil thickness after irradiations with 0.39 MeV Xe or 6 MeV Si ions at 293 K. The values are obtained with a diffraction vector along the <111> directions. Dotted lines are guides for the eyes.

In both cases, the loop density first increases with the irradiation fluence and their size is supposed to remain constant during this first stage. However, the loops appear and increase in number at a lower damage level for the Si irradiation (0.005 dpa) than for the Xe irradiation (0.07 dpa). For a given dpa value, the loop density after the Si irradiation is higher than the one measured after the Xe irradiation. For example, at about 0.07 dpa, the dislocation loops densities are $(24.1 \pm 5.0) \times 10^{15}$ and $(0.27 \pm 0.10) \times 10^{15}$ loops/cm^3 for the Si and Xe irradiations, respectively. For the Si irradiation, a loop growth and a transition from loops to lines should be observed for fluences higher than 3×10^{14} Si/cm², as for the Xe irradiation. A delay for this second stage could also be expected. However, high fluences are needed to reach this stage with the Si ion beam and it was not possible because of a lack of time. In addition, that was not the aim of this study. These results tend to indicate that the interaction between the incident ion and the crossed matter induces different kinetics of the loop evolution as a function of the electronic deposited energy.

3.2. Coupled effect of the electronic and the nuclear energy losses: sequential and dual ion beam irradiations

3.2.1. Effect of the Si ion beam on a pre-damaged sample (Xe then Si)

Sequential irradiation (Xe then Si) is performed to study the ionization effect on pre-existing defects in UO_2 thin foils (fig. 7). An unirradiated thin foil was pre-irradiated at 5×10^{14} Xe/cm^2 with 0.39 MeV Xe ions and then, irradiated at 3×10^{14} Si/cm^2 with 6 MeV Si ions.

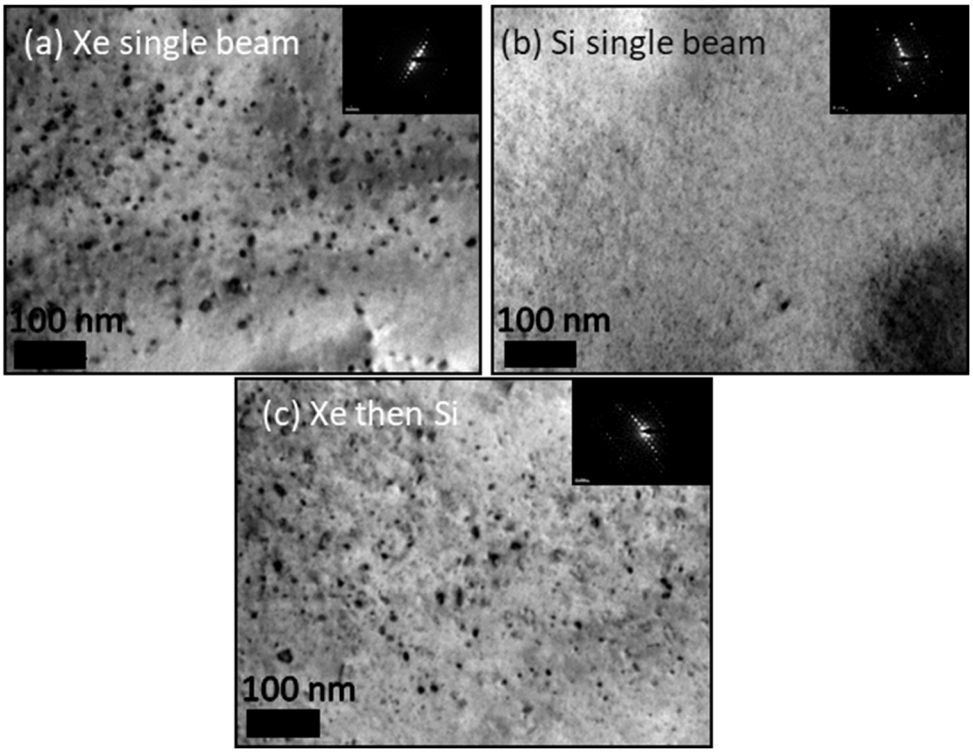

Figure 7: BF TEM micrographs of polycrystalline UO_2 thin foil irradiated at 293 K at (a) 5×10^{14} Xe/cm² with 0.39 MeV Xe ions, (b) 3×10^{14} Si/cm² with 6 MeV Si ions and (c) pre-damaged sample at 5×10^{14} Xe/cm² and then irradiated at 3×10^{14} Si/cm² (Xe then Si). The insets show the corresponding diffraction patterns along the <111> directions.

Many well-defined dislocation loops (~ 2×10^{16} loops/cm^3), of a mean size close to 7 nm, are present after irradiation with 0.39 MeV Xe ions at a fluence of 5×10^{14} Xe/cm² (Fig.7(a)), as presented in detail in part 3.1.1. Only very few little loops are revealed in fig. 7(b) after the 6 MeV Si irradiation at a fluence of 3×10^{14} Si/cm², highlighting the limited extended defect creation by the Si ion beam at this fluence (see part 3.1.2). After the Xe then Si irradiations (at the fluences above), no significant microstructural evolution is observed (fig. 7(c)). The loop density generated by the 0.39 Xe ion beam (about 2×10^{16} loops/cm^3) is not modified by the 6 MeV Si ion beam (same observed density). In addition, no mean size change is pointed out. These results will be further discussed in part 4.

3.2.2. Effect of dual ion beam irradiation (Xe & Si)

The results obtained for 0.39 MeV Xe irradiation are compared to those obtained with the simultaneous irradiation with 0.39 MeV Xe and 6 MeV Si ion beams (Xe & Si). The ratio between the Si and the Xe ions flux is set to 2. Electronic energy deposition in the thin foil is dominant over atomic energy deposition under the 6 MeV Si irradiation (Table 1). But, to limit the loops formation in the thin foil by this ion beam, the maximum used Si fluence is 2×10^{14} Si/cm². Fig.7 presents the micrographs obtained during the simultaneous irradiation (Xe&Si) for different steps.

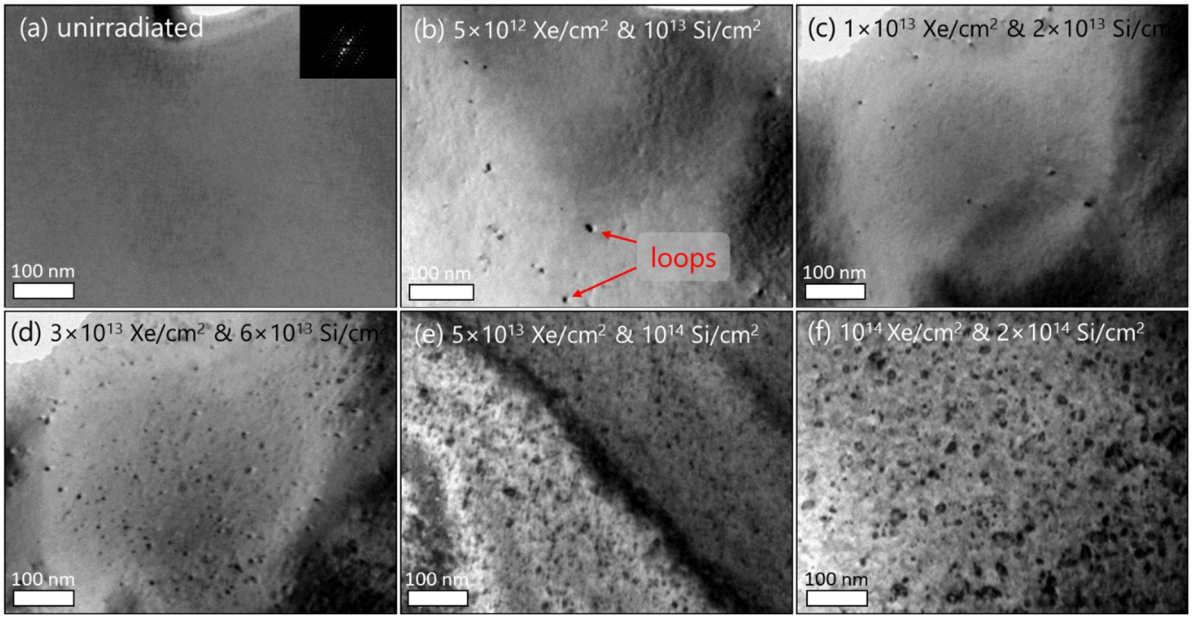

Figure 8 : BF TEM micrographs of polycrystalline UO_2 thin foil irradiated at 293 K with dual ion beam (Xe&Si) : (a) before irradiation, (b) at 5×10¹² Xe/cm² and 1×10¹³ Si/cm², (c) at 1×10¹³ Xe/cm² and 2×10¹³ Si/cm², (d) at 3×10¹³ Xe/cm² and 6×10¹³ Si/cm², (e) at 5×10¹³ Xe/cm² and 1×10¹⁴ Si/cm², and (f) at 1×10¹⁴ Xe/cm² and 2×10¹⁴ Si/cm². The insets show the corresponding diffraction patterns (g = 111 reflections).

The lamella microstructure before irradiation shows no observable defects (Fig. 8(a)). At the first fluence step (i.e. 5×10¹² Xe/cm² and 1×10¹³ Si/cm²), small dislocation loops are revealed (Fig. 8(b)). With the fluence increase (up to a fluence of 5×10¹³ Xe/cm²), the loop number increases (Fig. 8(b-e)). Beyond this fluence, the loops start to grow significantly (Fig. 8(f)).

Fig. 9 presents the loop repartition at the various fluences for the dual-beam irradiation (Xe&Si).

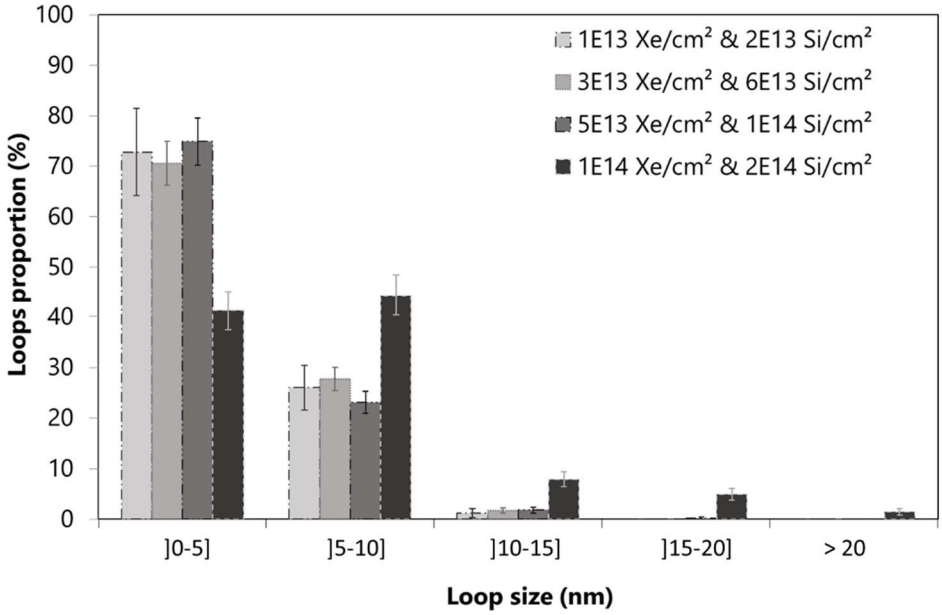

Figure 9: Repartition of the dislocation loop size at the various fluences, induced by dual beam irradiation with 0.39 MeV Xe and 6 MeV Si at 293 K. The lowest fluence (5×10¹² Xe.cm⁻²) are not represented here due to the low number of considered loops at this fluence.

For fluences ranging between 1×10^{13} and 5×10^{13} Xe/cm², the loop proportion, whose size is lower than 10 nm, remains constant (~ 73 ± 4 %). Between 0.5 and 1×10^{14} Xe/cm², an increase of the number of the medium-sized loops (]5-10] and]10-15] nm)(from (24.9 ± 2.6) % to (52.3 ± 5.5) %) as well as a decrease of the number of the smallest loops (from (74.9 ± 4.7) % to (41.3 ± 3.9) % for a size lower than 5 nm) is highlighted. In addition, new classes of larger loops ((5.4 ± 1.7) % of size ranging between]15-20] and > 20 nm) also appear at this fluence.

The final microstructure of the thin foil subjected to the Xe & Si irradiation (fig. 8(f)) is very different from the one subjected to single ion beam irradiation (Fig. 2(c)). It shows many large dislocation loops as illustrated on the Fig. 10(b). We also observed some discrepancies in the loop density evolution (Fig. 10(a)). The dislocation loop density for the dual-beam irradiation, exhibits the same evolution with the fluence increase as all the other single irradiations (Fig.10): (1) Small loops are formed continuously after the first few irradiation seconds (i.e. after 5×10^{12} Xe/cm²), (2) the dislocation loops with a constant mean size increase in density, then (3) they begin to grow when their density saturates.

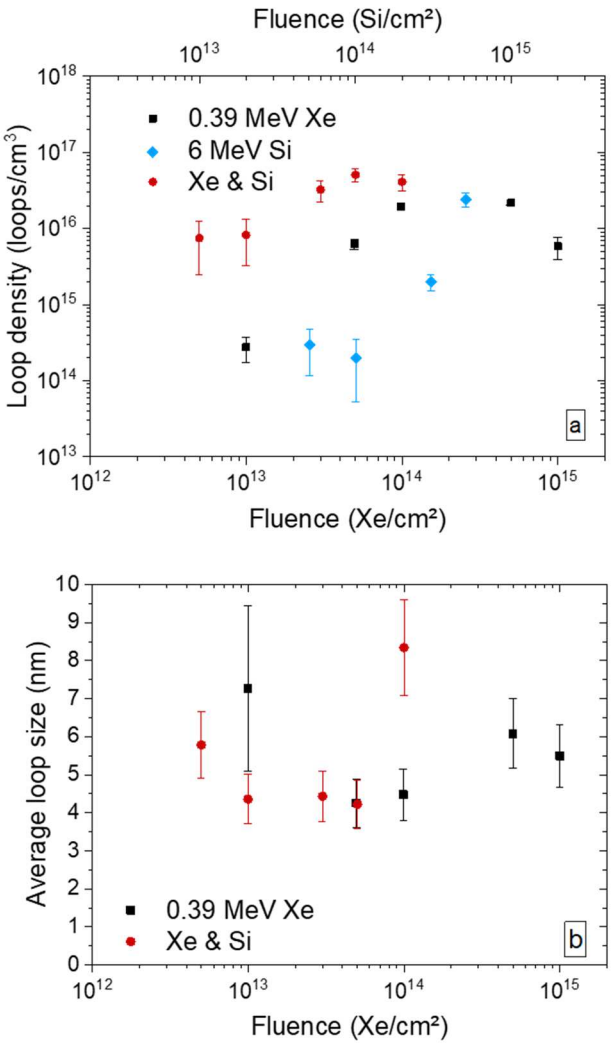

Figure 10: Evolution of (a) dislocation loop density and (b) loop size as a function of the fluence for the irradiations with 0.39 MeV Xe and 6 MeV Si at 293 K and for the dual-beam irradiation (Xe & Si). The represented values are obtained with a diffraction vector along the <111> direction. Dotted lines in (a) are guide for the eyes.

We observed some discrepancies between the single Xe and the Xe & Si irradiation. It seems that, for the simultaneous irradiation, the loops appear at a slightly lower fluence. The first dislocation loops are observed at a lower Xe fluence (5×10^{12} Xe/cm²) for the Xe&Si irradiation

compared to the single Xe irradiation (1×10^{13} Xe/cm^2). At 1×10^{13} Xe/cm^2, a larger loops density is highlighted for the Xe & Si (40 times larger than for the Xe irradiation) (fig.10(a)). It appears that the loop density for the Xe & Si irradiation is not equal to the sum of loops density obtained for the two single beam irradiations (Xe and Si). It highlights that the simultaneous irradiation is not a simple accumulation of the induced loops by the single ion beams. We observe a saturation of the loop density at a fluence of 5×10^{13} Xe/cm^2 (and 1×10^{14} Si/cm^2). This stabilization occurs at a lower fluence compared to the single Xe irradiation (1×10^{14} Xe/cm^2) or the single Si irradiation (fluence not reached during our irradiation).

The loop size evolves slightly differently between dual and single ion beam irradiations (Fig.10(b)). For the Xe irradiation, the loops did not appear to grow significantly up to 1×10^{14} Xe/cm². Between 1 and 5×10^{14} Xe/cm², the loops begin to grow. By contrast, concerning the Xe & Si irradiation, the loops start to grow earlier, between 0.5 and 1×10^{14} Xe/cm².

In summary, it is worth noting that the evolution mechanisms of extended defects are similar whatever the irradiation conditions. However, the Si 6 MeV ion beam seems to affect the kinetics of extended defects evolution during the dual beam irradiation, thereby accelerating the loop nucleation and hence their growth. The average loop size and the loop density are larger for the dual-beam irradiation than for the single Xe ion beam irradiation at a given fluence.

4. Discussion

The UO_2 modifications induced by low- and high-energy ions was studied by *in situ* transmission electron microscopy. The dislocation loop evolution was determined under sequential and simultaneous ion beam irradiations. The irradiation with 6 MeV Si ions of a pre-damaged sample with 0.39 MeV Xe ions (Xe then Si) does not induce an evolution of the dislocation loops in term of density and size, whereas the microstructure is completely different when the Xe and Si ions beams are used simultaneously (Xe & Si). Indeed, the density and the size of the dislocation loops are higher after the Xe & Si irradiation compared to the Xe irradiation for a given Xe fluence.

Such a difference can be attributed to the experimental procedure: sequential or simultaneous irradiations. As there is no time and space correlation between the low- and high-energy ions, the dual beam irradiation is likely the result of the overlap of multiple sequential irradiations (of low fluence steps). The microstructure just damaged by a given low-energy ion is then submitted to the irradiation of a high-energy ion arriving later without the necessity of time overlap between both trajectories. Thus, in the case of the Xe & Si irradiation, the disorder reached by the Xe ion at the irradiation beginning is very low when the Si ion interacts with this latter, so that high-velocity ion irradiation may induce more easily damage annealing (recombination, absorption by other clusters…). It is important to note that the low-energy ions induce continuously ballistic damage. Thus, Si ions will still interact with small defects and, for higher fluence, also with extended defects. On the contrary, in the case of sequential irradiation, the Si ions interact with a high density of dislocation loop already well-formed. Consequently, in this case, the subsequent Si ion irradiation will be unable to modify significantly the microstructure. This is supported by the studies performed on Si and SiC samples submitted to dual ion beam irradiations (15-41). By tailoring the flux ratio between low- and high-energy ion beams, it has been shown that the effect of the high-energy ion beam on a pre-damaged structure depends on the initial disorder level. Thus, depending on the defect kind (isolated point defects, cluster of point defects, or extended one) present in the material, one given high-energy ion beam will have an influence or not on the microstructure

evolution. The electronic energy transfer in the Si irradiation is insufficient to induce a microstructural evolution for high damage structure (during sequential irradiation) but may affect the microstructure during simultaneous irradiation (it interacts only with small defects).

Furthermore, when the experimental conditions are gathered (only during dual-beam irradiation in this case), we clearly observe a coupled effect between nuclear and electronic energy loss. The extended defect evolution is similar for the Xe and Xe & Si irradiations: (i) continuous small loop formation (around 4 nm), (ii) dislocation loops increase in terms of density, (iii) then the loop density saturates and the dislocation size begins to increase. However, those phenomena seem to be accelerated for the Xe & Si irradiation due to the electronic excitations generated by the Si ions along their path. To estimate the local heating induced along the Si ion path due to the electronic energy deposition, calculations with the unified thermal spike model were carried out [39–41]. This model has been developed to account for mid-range ion energy, in which the temperature increase is calculated before reaching the melting temperature. The calculations details and used parameters can be found in [26]. However, this model was developed to calculate the thermal energy distribution for predominant electronic energy losses. In our case, nuclear energy losses are not completely negligible. Thus, iTS calculations can only give an order of magnitude of the reached temperature, not an absolute value. An increase of about 873 K is evaluated in a radius of about 2 nm in the vicinity of the Si ion path which lasts a maximum of about 5 ps. As the microstructure evolves during the Xe & Si irradiation, but not after the Xe then Si irradiation, the local temperature increase may induce rather the mobility of some point defects but is not high enough to anneal bigger defect clusters, such as dislocation loops of around 4 nm. The increased-mobility of small defects could explain the higher loop density at the beginning of the irradiation observed for the Xe & Si irradiation. Point defects could easier clustering in new dislocation loops and/or be absorbed by defect clusters already present but too small to be detected using the TEM. It is important to note that in our experiments, we see only clusters of diameter larger than about 1-2 nm (depending on the thin foil quality). Smaller clusters probably exist but cannot be observed directly. This is supported by the CMD simulations, for irradiations at a temperature higher than 700 K, which have displayed higher mobility of point defects leading to a rise of clustered interstitials [42]. This clustering conducts then to an accelerated loop nucleation. Thus, the ionizations along the 6 MeV Si ion path might accelerate the formation of dislocation loops as it occurs with a raise of the irradiation temperature [3, 7]. When the loop density saturates (earlier in the case of Xe & Si irradiation), an acceleration of the dislocation loop growth during the Xe & Si irradiation is highlighted, and could also be explained by an increase of the point defect mobility. These point defects could be more easily absorbed by dislocation loops, inducing an enhanced loop growth due to the temperature effect.

To support this assumption, we compared these results with our previous work on 0.39 MeV Xe irradiation performed at 873 K [3] on fig. 11. It appears very clearly that data obtained for the Xe & Si irradiation match quite well with data obtained at 873 K in terms of density. The loop size growth seems to be even more efficient in the case of dual-beam than for irradiation performed at 873 K.

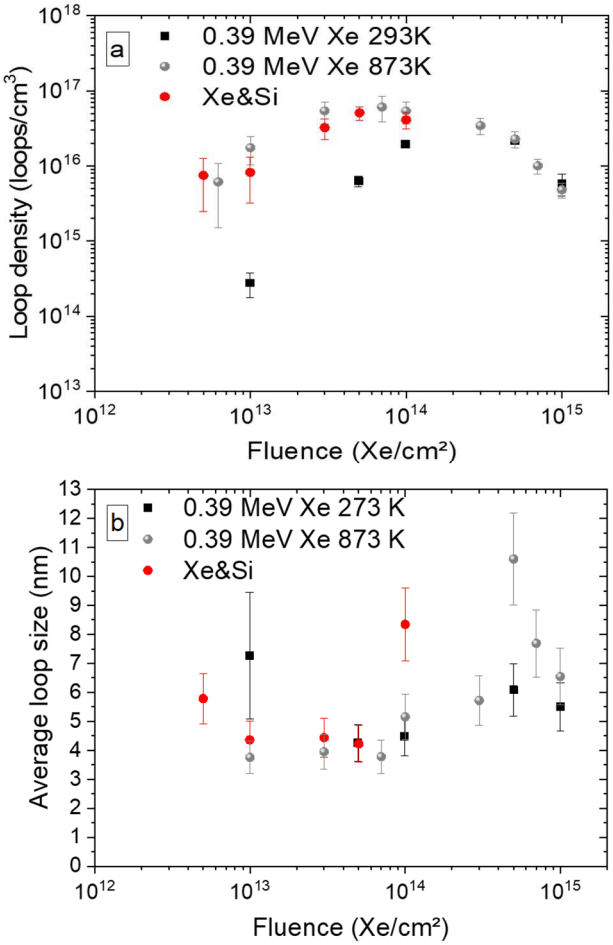

Figure 11: Dislocation loops evolution as a function of fluence for 0.39 MeV Xe irradiation at 293 K (this study), 873 K [3], and for Xe&Si irradiation at 293 K (this study).

All of these observations are consistent with our previous study, which has shown a transformation of dislocation loops into lines at a lower damage level for dual ion beam irradiation than for the corresponding single ion beam irradiation [26]. However, the coupled effect of ballistic and electronic energy losses was higher than in the present paper due to the more important electronic energy loss of the high-energy ion (12 keV/nm). The influence of this parameter will be discussed in a future paper.

5. Conclusions

Ion beam irradiations were performed to investigate the coupled effect between electronic and nuclear energy deposition in UO_2. *In situ* TEM observations were carried out to follow the evolution of dislocation loops during four kinds of irradiations. Single ion beam irradiations were performed at room temperature to favor either the nuclear (0.39 MeV Xe) or the electronic (6 MeV Si) damage. The effect of electronic ionizations in a pre-damaged sample with Xe ions was investigated (Xe then Si). In addition, the microstructure evolution under a simultaneous irradiation (Xe & Si) was studied. It appears that the extended defects evolution is quite similar for the low-energy or dual-beam irradiations. Small loops first continuously nucleate. With the irradiation fluence increase, the density of dislocation loops increases up to reach a saturation.

The dislocations loops then begin to grow. However, in the case of the dual beam irradiation, all these phenomena occur at lower values of damage level. Thus, the electronic energy deposited to the target (~ 6 keV/nm) modifies the kinetics of extended defects evolution due to a low temperature non-melting thermal spike, which induced locally (2 nm around the ion path) a temperature of 873 K. However, the subsequent irradiation of 6 MeV Si ions does not affect the dislocation loops already formed, but likely only the mobility of point defects. No evolution of the loop size or the loop density is therefore noticed in the Xe then Si irradiations.

This study shows that, for one given high-energy ion beam, a microstructure evolution can occur depending on the kind of defects (point defects, small clusters, or extended defects) are present in the material. The increase of electronic stopping power may induce a larger effect for example on the extended defects. Future works will aim at characterizing this last point by varying the ion energy during dual-beam irradiation.

Acknowledgments

Experiments performed at the CSNSM facility: JANNuS-Orsay (CSNSM, Univ Paris-Sud, CNRS/IN2P3, Orsay, France). This experiment was supported by the EMIR French accelerator network.

References

[1] L. F. He, J. Pakarinen, M. A. Kirk, J. Gan, A. T. Nelson, X.-M. Bai, A. El-Azab, and T. R. Allen, 'Microstructure evolution in Xe-irradiated UO2 at room temperature', *Nucl. Instrum. Methods Phys. Res. Sect. B-Beam Interact. Mater. Atoms*, 330 (2014) 55–60.

[2] L. He, M. Gupta, C. A. Yablinsky, J. Gan, M. A. Kirk, X.-M. Bai, J. Pakarinen, and T. Allen, 'In situ TEM observation of dislocation evolution in Kr-irradiated UO2 single crystal', *Journal of Nuclear Materials*, 443 (2013) 71–77.

[3] C. Onofri, C. Sabathier, C. Baumier, C. Bachelet, H. Palancher, B. Warot-Fonrose, and M. Legro, 'Influence of exogenous xenon atoms on the evolution kinetics of extended defects in polycrystalline UO2 using in situ TEM', *J. Nucl. Mater.*, 512 (2018) 297–306.

[4] C. Sabathier, G. Martin, A. Michel, G. Carlot, S. Maillard, C. Bachelet, F. Fortuna, O. Kaitasov, E. Olivier, and P. Garcia, 'In-situ TEM observation of nano-void formation in UO2 under irradiation', *Nucl. Instrum. Methods Phys. Res. Sect. B-Beam Interact. Mater. Atoms*, 326 (2014) 247–250.

[5] A. Michel, C. Sabathier, G. Carlot, O. Kaitasov, S. Bouffard, P. Garcia, and C. Valot, 'An in situ TEM study of the evolution of Xe bubble populations in UO2', *Nucl. Instrum. Methods Phys. Res. Sect. B-Beam Interact. Mater. Atoms*, 272 (2012) 218–221.

[6] L. F. He, B. Valderrama, A.-R. Hassan, J. Yu, M. Gupta, J. Pakarinen, H. B. Henderson, J. Gan, M. A. Kirk, A. T. Nelson, M. V. Manuel, A. El-Azab, and T. R. Allen, 'Bubble formation and Kr distribution in Kr-irradiated UO2', *Journal of Nuclear Materials*, 456 (2015) 125–132.

[7] C. Onofri, C. Sabathier, C. Baumier, C. Bachelet, H. Palancher, and M. Legros, 'Evolution of extended defects in polycrystalline Au-irradiated UO2 using in situ TEM: Temperature and fluence effects', *J. Nucl. Mater.*, 482 (2016) 105–113.

[8] C. Onofri, C. Sabathier, G. Carlot, D. Drouan, C. Bachelet, C. Baumier, M. Gérardin, and M. Bricout, 'Changes in voids induced by ion irradiations in UO2: In situ TEM studies', *Nuclear Instruments and Methods in Physics Research Section B: Beam Interactions with Materials and Atoms*, 463 (2020) 76–85.

[9] K. Nogita, K. Hayashi, K. Une, and K. Fukuda, 'Depth profiles of damage accumulation in UO2 and (U,Gd)O2 pellets irradiated with 100 MeV iodine ions', *Journal of Nuclear Materials*, 273 no. 3 (1999) 302–309.

[10] N. Ishikawa, T. Sonoda, T. Sawabe, H. Sugai, and M. Sataka, 'Electronic stopping power dependence of ion-track size in UO2 irradiated with heavy ions in the energy range of similar to 1 MeV/u', *Nucl. Instrum. Methods Phys. Res. Sect. B-Beam Interact. Mater. Atoms*, 314 (2013) 180–184.

[11] V. V. Pisarev and S. V. Starikov, 'Atomistic simulation of ion track formation in UO2', *J. Phys.-Condes. Matter*, 26 no. 47 (2014) 475401.

[12] F. Garrido, C. Choffel, J.-C. Dran, L. Thome, L. Nowicki, and A. Turos, 'Structural modifications in uranium dioxide irradiated with swift heavy ions', *Nuclear Instruments and Methods in Physics Research Section B: Beam Interactions with Materials and Atoms*, 127–128 (1997) 634–638.

[13] T. Wiss, Hj. Matzke, C. Trautmann, M. Toulemonde, and S. Klaumünzer, 'Radiation damage in UO2 by swift heavy ions', *Nuclear Instruments and Methods in Physics Research Section B: Beam Interactions with Materials and Atoms*, 122 no. 3 (1997) 583–588.

[14] K. Hayashi, H. Kikuchi, and K. Fukuda, 'Radiation damage of UO2 by high-energy heavy ions', *J. Nucl. Mater.*, 248 (1997) 191–195.

[15] L. Thome, G. Velisa, S. Miro, A. Debelle, F. Garrido, G. Sattonnay, S. Mylonas, P. Trocellier, and Y. Serruys, 'Recovery effects due to the interaction between nuclear and electronic energy losses in SiC irradiated with a dual-ion beam', *J. Appl. Phys.*, 117 no. 10 (2015) 105901.

[16] Y. Zhang, R. Sachan, O. H. Pakarinen, M. F. Chisholm, P. Liu, H. Xue, and W. J. Weber, 'Ionization-induced annealing of pre-existing defects in silicon carbide', *Nat. Commun.*, 6 (2015) 8049.

[17] A. Debelle, M. Backman, L. Thome, W. J. Weber, M. Toulemonde, S. Mylonas, A. Boulle, O. H. Pakarinen, N. Juslin, F. Djurabekova, K. Nordlund, F. Garrido, and D. Chaussende, 'Combined experimental and computational study of the recrystallization process induced by electronic interactions of swift heavy ions with silicon carbide crystals', *Phys. Rev. B*, 86 no. 10 (2012) 100102.
[18] A. H. Mir, S. Peuget, M. Toulemonde, P. Bulot, C. Jegou, S. Miro, and S. Bouffard, 'Defect recovery and damage reduction in borosilicate glasses under double ion beam irradiation', *EPL*, 112 no. 3 (2015) 36002.
[19] K. Jin, Y. Zhang, and W. J. Weber, 'Synergistic effects of nuclear and electronic energy deposition on damage production in KTaO3', *Materials Research Letters*, 6 no. 9 (2018) 531–536.
[20] L. Thome, G. Velisa, A. Debelle, S. Miro, F. Garrido, P. Trocellier, and Y. Serruys, 'Behavior of nuclear materials irradiated with a dual ion beam', *Nucl. Instrum. Methods Phys. Res. Sect. B-Beam Interact. Mater. Atoms*, 326 (2014) 219–222.
[21] Y. Zhang, X. Wang, S. Liu, M. Tang, and Z. Zhao, 'Characterisation of dual ion beam irradiated yttria-stabilised zirconia by specific analytical techniques', *Nuclear Instruments and Methods in Physics Research Section B: Beam Interactions with Materials and Atoms*, C no. 342 (2015) 52–61.
[22] L. Thome, G. Gutierrez, I. Monnet, F. Garrido, and A. Debelle, 'Ionization-induced annealing in silicon upon dual-beam irradiation', *Journal of Materials Science*, (2020).
[23] B. Marchand, N. Moncoffre, Y. Pipon, N. Bererd, C. Garnier, L. Raimbault, P. Sainsot, T. Epicier, C. Delafoy, M. Fraczkiewicz, C. Gaillard, N. Toulhoat, A. Perrat-Mabilon, and C. Peaucelle, 'Xenon migration in UO2 under irradiation studied by SIMS profilometry', *J. Nucl. Mater.*, 440 no. 1–3 (2013) 562–567.
[24] N. Djourelov, B. Marchand, H. Marinov, N. Moncoffre, Y. Pipon, N. Bererd, P. Nedelec, L. Raimbault, and T. Epicier, 'Study of temperature and radiation induced microstructural changes in Xe-implanted UO2 by TEM, STEM, SIMS and positron spectroscopy', *J. Nucl. Mater.*, 443 no. 1–3 (2013) 562–569.
[25] G. Gutierrez, D. Gosset, M. Bricout, C. Onofri, and A. Debelle, 'Effect of coupled electronic and nuclear energy deposition on strain and stress levels in UO2', *Journal of Nuclear Materials*, 519 (2019) 52–56.
[26] M. Bricout, C. Onofri, A. Debelle, Y. Pipon, R. C. Belin, F. Garrido, F. Leprêtre, and G. Gutierrez, 'Radiation damage in uranium dioxide: Coupled effect between electronic and nuclear energy losses', *Journal of Nuclear Materials*, 531 (2020) 151967.
[27] Hj. Matzke and A. Turos, 'Erratum: Surface damage in UO2 due to mechanical polishing and ion bombardment', *Journal of Nuclear Materials*, 114 no. 2 (1983) 349–352.
[28] A. J. Manley, 'Transmission electron microscopy of irradiated U02 fuel pellets', *Journal of Nuclear Materials*, 27 no. 2 (1968) 216–224.
[29] R. F. Egerton, '*Electron Energy-Loss Spectroscopy in the Electron Microscope*'. Springer Science & Business Media (2011).
[30] C. Degueldre, R. Schaeublin, J. Krbanjevic, and E. Minikus, 'Electron energy loss spectroscopy investigation through a nano ablated uranium dioxide sample', *Talanta*, 106 (2013) 408–413.
[31] H.-R. Zhang, R. F. Egerton, and M. Malac, 'Local thickness measurement through scattering contrast and electron energy-loss spectroscopy', *Micron*, 43 no. 1 (2012) 8–15.
[32] A. Gentils and C. Cabet, 'Investigating radiation damage in nuclear energy materials using JANNuS multiple ion beams', *Nuclear Instruments and Methods in Physics Research Section B: Beam Interactions with Materials and Atoms*, 447 (2019) 107–112.
[33] J. F. Ziegler, M. D. Ziegler, and J. P. Biersack, 'SRIM - The stopping and range of ions in matter (2010)', *Nucl. Instrum. Methods Phys. Res. Sect. B-Beam Interact. Mater. Atoms*, 268 no. 11–12 (2010) 1818–1823.
[34] J. Soullard, 'High-Voltage Electron-Microscope Observations of UO2', *J. Nucl. Mater.*, 135 no. 2–3 (1985) 190–196.

[35] C. Meis and A. Chartier, ‘Calculation of the threshold displacement energies in UO2 using ionic potentials’, *J. Nucl. Mater.*, 341 no. 1 (2005) 25–30.
[36] C. Sabathier, L. Vincent, P. Garcia, F. Garrido, G. Carlot, L. Thome, P. Martin, and C. Valot, ‘In situ TEM study of temperature-induced fission product precipitation in UO2’, *Nucl. Instrum. Methods Phys. Res. Sect. B-Beam Interact. Mater. Atoms*, 266 no. 12–13 (2008) 3027–3032.
[37] C. Onofri, M. Legros, J. Lechelle, H. Palancher, C. Baumier, C. Bachelet, and C. Sabathier, ‘Full characterization of dislocations in ion-irradiated polycrystalline UO2’, *J. Nucl. Mater.*, 494 (2017) 252–259.
[38] B. Ye, M. A. Kirk, W. Chen, A. Oaks, J. Rest, A. Yacout, and J. F. Stubbins, ‘TEM investigation of irradiation damage in single crystal CeO2’, *J. Nucl. Mater.*, 414 no. 2 (2011) 251–256.
[39] M. Toulemonde, W. Assmann, Y. Zhang, M. Backman, W. J. Weber, C. Dufour, and Z. G. Wang, ‘Material transformation: Interaction between nuclear and electronic energy losses’, in *2nd International Summer School on Nuclear Glass Wasteform: Structure, Properties and Long-Term Behavior (sumglass 2013)*. Amsterdam: Elsevier Science Bv (2014) 272–277.
[40] M. Toulemonde, W. J. Weber, G. Li, V. Shutthanandan, P. Kluth, T. Yang, Y. Wang, and Y. Zhang, ‘Synergy of nuclear and electronic energy losses in ion-irradiation processes: The case of vitreous silicon dioxide’, *Phys. Rev. B*, 83 no. 5 (2011) 054106.
[41] H. D. Mieskes, W. Assmann, F. Gruner, H. Kucal, Z. G. Wang, and M. Toulemonde, ‘Electronic and nuclear thermal spike effects in sputtering of metals with energetic heavy ions’, *Phys. Rev. B*, 67 no. 15 (2003) 155414.
[42] G. Martin, C. Sabathier, J. Wiktor, and S. Maillard, ‘Molecular dynamics study of the bulk temperature effect on primary radiation damage in uranium dioxide’, *Nucl. Instrum. Methods Phys. Res. Sect. B-Beam Interact. Mater. Atoms*, 352 (2015) 135–139.